

Focal Mechanism Determination and Propagation Characteristics of High-frequency S-waves on the Tibetan Plateau

L. Zhu and D. V. Helmberger
California Institute of Technology
Contract No. F19628-95-C-0096

July 29, 1995

Abstract

One of the most useful regional discriminants is the ratio of short-period S/P energy, on the basis that nuclear explosions tend to have less S energy than earthquakes at high frequencies. However, the high-frequency S waves from earthquakes can also be easily blocked or attenuated during the propagation, especially along the boundaries between different tectonic regions and within tectonic active areas. So, an essential understanding of the regional crustal structures and associated wave propagation characteristics are needed before establishing effective discrimination methods for that area. In this report, we first determined the crustal structure of the Tibetan Plateau and the focal mechanisms of regional events recorded during the 1991-1992 Tibet passive recording experiment. In particular, we improve the source mechanism estimation technique proposed by Zhao and Helmberger (1994) by introducing a distance range scaling factor. This helps to constrain the source orientation by fully utilizing the radiation patterns contained in the different portions of the whole 3-component records. By apply the method to the regional events of the Tibet Plateau, we obtained the focal depths and mechanisms. Most events are found to be shallower than 20 km. However, we also identified 3 subcrustal events (at depth of 70-80 km) under the Himalayan Thrust Belt and the Indus Zangbo suture zone. Their mechanisms are quite different from those of shallow events in the same region.

We find that the radiation pattern of P and S behave quite well as a function of frequency below 1 Hz. At frequencies above 3 Hz, the amplitudes vary strongly from station to station. High attenuation of short-period S waves is found for ray paths through the north-central plateau. This is consistent with previously observed inefficient propagation of high frequency S_n in this area. It also correlates with the young volcanisms and low crustal velocities and P_n velocities. The variation of energy ratio of short-period SH component vs. broadband SH component with distance range are modeled by reducing Q values in the lower crust. Combining with other observations, we suggest that there is a hot, possibly partially melted lower crust in the north-central Tibet.

Focal Mechanism Determination and Propagation Characteristics of High-frequency S-waves on the Tibetan Plateau

1 OBJECTIVE

Our objective is to investigate the propagation characteristics of broadband and high-frequency S-waves on the Tibetan Plateau. Regional crustal structure and the focal mechanisms are determined by analyzing broadband waveform data obtained during the 1991-1992 passive recording experiment (Owens et al., 1993). In particular, we improve the source mechanism estimation technique proposed by Zhao and Helmberger (1994) by introducing a distance range scaling factor. This helps to constrain the source orientation by fully utilizing the radiation patterns contained in the different portions of the whole 3-component records.

2 RESEARCH ACCOMPLISHED

2.1 Introduction

One of the most useful regional discriminants is the ratio of short-period S/P energy, on the basis that nuclear explosions tend to have less S energy than earthquakes at high frequencies. However, the high-frequency S waves from earthquakes can also be easily blocked or attenuated during the propagation, especially along the boundaries between different tectonic regions and within tectonic active areas. So, an essential understanding of the regional crustal structures and associated wave propagation characteristics are needed before establishing effective discrimination methods for that area.

The Tibetan Plateau is the youngest plateau in the world. It is estimated that the present elevation of much of the plateau was attained by about 8 million years ago (Harrison et al., 1992). The plateau is surrounded by several old platforms and shields with large-scale thrust faults and strike-slip faults serving as boundaries. Even within the plateau, structural heterogeneities exist. For example, by using the short-period records of shallow events of Tibet and vicinity at WSSN stations in India and Pakistan, Ni and Barazangi (1983) identified a zone of inefficient Sn propagation in the north-central Tibet. Together with the evidence of young volcanism found in the same area and the low crustal and upper-mantle velocities from surface wave dispersion analysis, Molnar suggests the existence of a partial melting uppermost mantle under north-central Tibet (Molnar, 1988).

Recent PASSCAL experiment on the Tibet Plateau (see Owens et al., 1993) provided a new data set in this area. For the first time, broadband regional waveforms are available with both the events and receivers inside the plateau. In this report, we use this data set to calibrate the regional crustal structure model, determine the focal depths and mechanisms of regional events, and investigate the propagation characteristics of high frequency S-waves on the plateau.

2.2 1-D Crustal model of the Tibetan Plateau

Several events occurred with the array (Figure 1) were used to calibrate the regional crustal model. From their broadband displacement records, major crustal phases such as Pn, Sn, PmP, SmS can be identified and provide constraints on the velocities of lower crust and uppermost mantle. Waveforms of regional Love wave are used to constrain the upper crustal velocity. Our best 1-D crustal model is shown in Table 1. It consists of a main crustal layer of 60 km thick with a 4 km layer on top of it. Note the lower crustal shear velocity (3.5 km/s) and higher crustal V_p/V_s ratio, which are also consistent with the teleseismic receiver function analysis (Zhu et al., 1993).

Table 1 Average velocity model of the Tibetan Plateau

layer	Thickness (km)	V_p (km/s)	V_s (km/s)
1	4	4.70	2.70
2	60	6.20	3.50
3	-	8.14	4.70

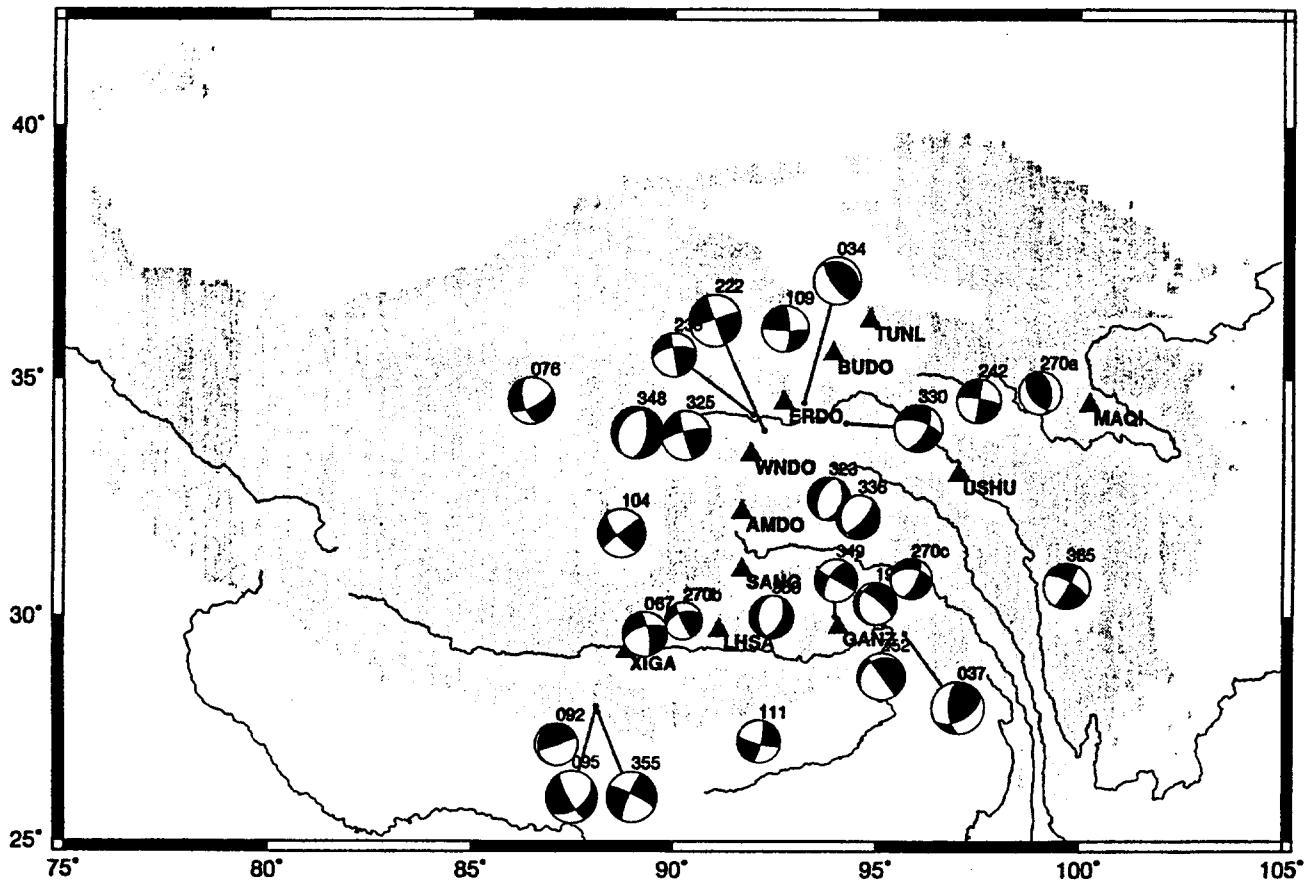


Figure 1: Broadband stations of 1991-1992 Tibet experiment. Shading indicates elevation above 3 km. Source mechanisms are determined from the broadband waveforms recorded at these stations (see text).

2.3 Improvement of source estimation technique

Zhao and Helmberger (1994) proposed a source mechanism estimation technique using regional broadband waveform data. The method applies a direct grid search in the source orientation parameter space for the minimum L1 and L2 norms of the difference between waveforms and synthetics. One of the advantages of

the method is that it desensitizes the timing between principal crustal arrivals by fitting portions of the waveforms independently, allowing some time shifts between the observation and synthetics. So, good source mechanism estimation can be obtained even when only imperfect Green's functions are available.

Since the Pnl portion of the waveform are much smaller in amplitude compared with the surface wave portion, and also because the procedure usually involves several station records at different distance ranges, the misfit error for each portion of the waveforms is defined as the norm of the discrepancy normalized by the norm of the data u and the synthetics f (Zhao and Helmberger, 1994):

$$e = \frac{\|u - f\|}{\|u\| \cdot \|f\|}, \quad (1)$$

such that all the portions of the data have similar weights in calculating the misfit between the observation and synthetics. However, in observations there are often some portions of the waveforms that are nodal. In that case, the grid search will fail since the norm of data and synthetic vanish. To overcome this problem, we introduce a distance range scaling factor and define the misfit error for record at distance range r as

$$e = \left\| \left(\frac{r}{r_0} \right)^p \cdot \|f - u\| \right\|, \quad (2)$$

here p is a scaling factor to give the record at r the same weight as that at reference distance r_0 . According to the propagation properties of the phases, an appropriate choice of p for body wave portion is $p = 1$, and for surface wave portion $p = 0.5$. The p -value could also be adjusted according to the actual amplitude attenuation in the studying area.

Figure 2a,b show the values of misfit errors defined by (1) and (2) as functions of the dip and rake of the source for a event in southern Tibet. The former one shows high peaks at the grids when synthetics is near nodal. The newly defined misfit error is much more well-behaved. It has the global minimum at (*strike* = 315, *dip* = 85, *rakke* = 255), but also shows three three local minimums (Figure 2b). In other words, the newly defined misfit error makes it easier to find the correct global minimum and estimate the uncertainties.

2.4 Focal mechanisms and depths of events in the plateau

We applied the improved source estimation technique to the regional events recorded during the one year experiment. The Green's functions are calculated using the 1D model (Table 1) at different depths. Figure 1 shows the low-hemisphere projection of focal mechanisms of the events we investigated. Randall et al (1995) estimated the moment tensors of most events from the long period waveforms of the same data set. Our results are similar theirs, although we analyzed 8 more events which are not included in Randall's solutions.

Most events are found to be shallower than 20 km. However, we also determined 3 events (event 355, 067, and 095 in Figure 1) to be deep, below the crust (Zhu and Helmberger, 1995). The existence of these intermediate depth events and their source mechanisms provided us important information about the temperature and stress in the upper mantle.

2.5 High frequency S-wave attenuation on the Tibet Plateau

The broadband waveform modeling shows that the radiation of P and S waves on the Tibet Plateau behaves quite well as a function of frequency below 1 Hz. Figure 3a shows tangential displacement records of event 222 compared to the synthetics. However, at frequencies above 3 Hz, the amplitudes vary strongly from station to station (Figure 3b). For example BUDO and AMDO are at similar distance ranges, but BUDO is located in the north-central plateau where high attenuation of high-frequency Sn were observed (Ni and Barazangi, 1983). Correspondingly, the high frequency amplitude at BUDO are much smaller than at AMDO. Same is true for station TUNL compared with SANG.

To characterize the propagation of high frequency S-waves within the plateau, we calculate the short-period S/P energy ratios for all the event-receiver paths within distance range between 320 to 1000 km. Figure 4 shows the results; the solid lines represent paths with a ratio of more than 0.6 and the dashed

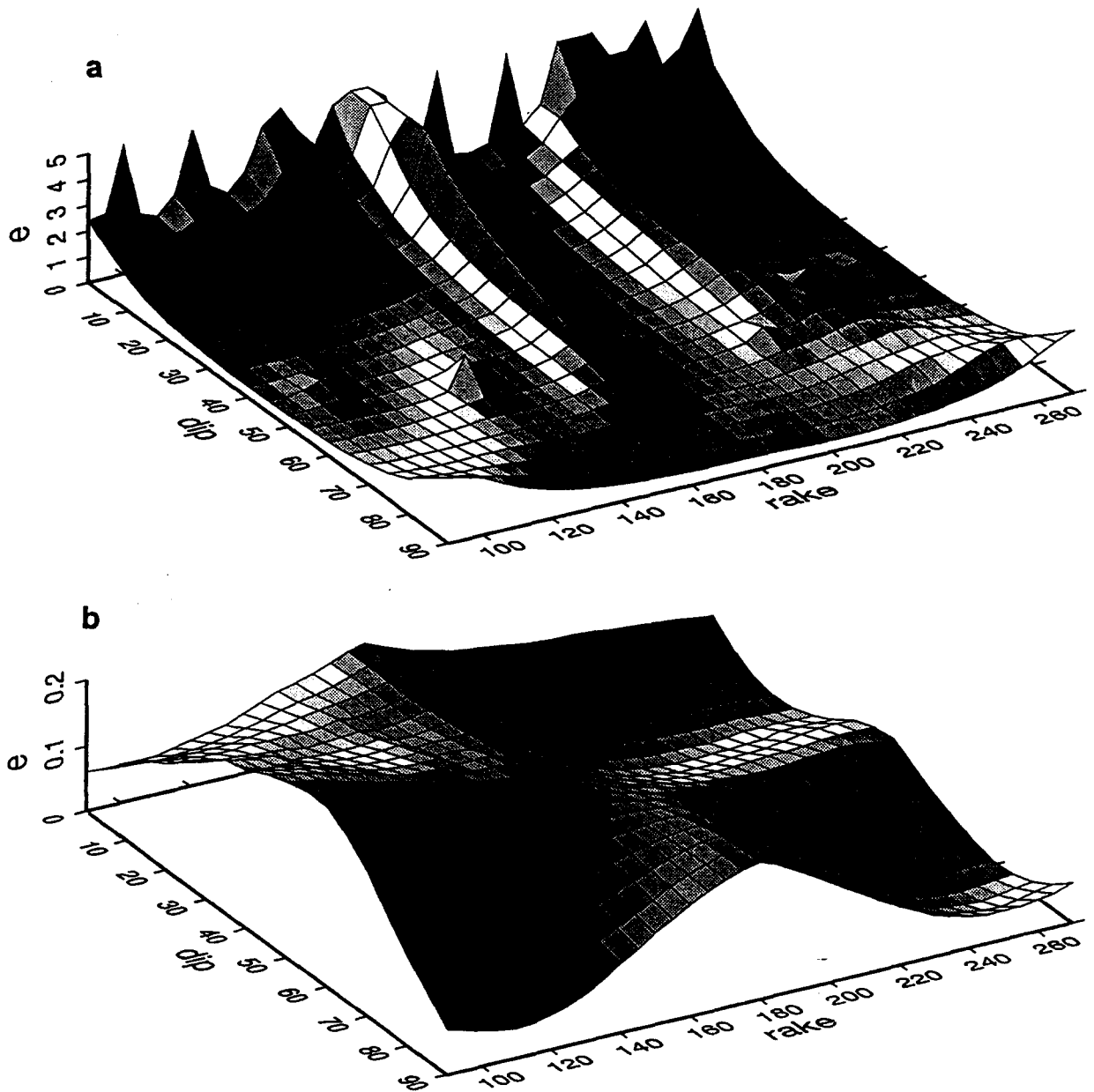


Figure 2: The waveform misfit errors as a function of dip and rake of the source orientation for one of the regional event (Event 199 in Figure 1). The strike is fixed at 315. a) The misfit error defined by Zhao and Helmberger (1994). b) Newly defined misfit error by introducing distance range scaling factor.

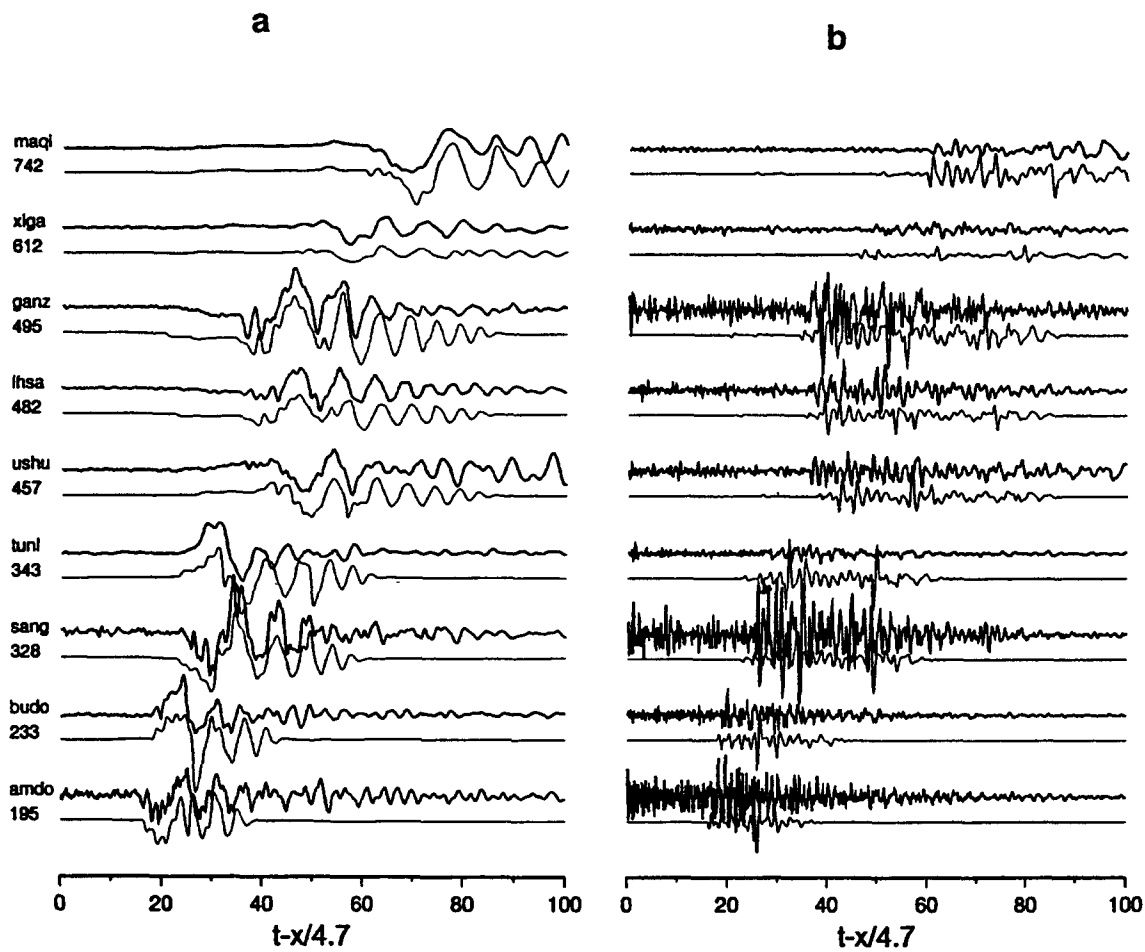


Figure 3: Broadband (a) and short-period (b) tangential displacements of event 222 (focal depth at 10 km). Thin lines are corresponding synthetics with source mechanisms obtained from the grid search. True amplitudes are plotted with distance range scaling factor $p = 0.5$ for (a) and $p = 2$ for (b)

lines correspond to paths with a ratio of less than 0.4. The high-frequency S-waves can propagate efficiently in southeastern Tibet and north of the Plateau, but have difficulty propagating through the north-central plateau.

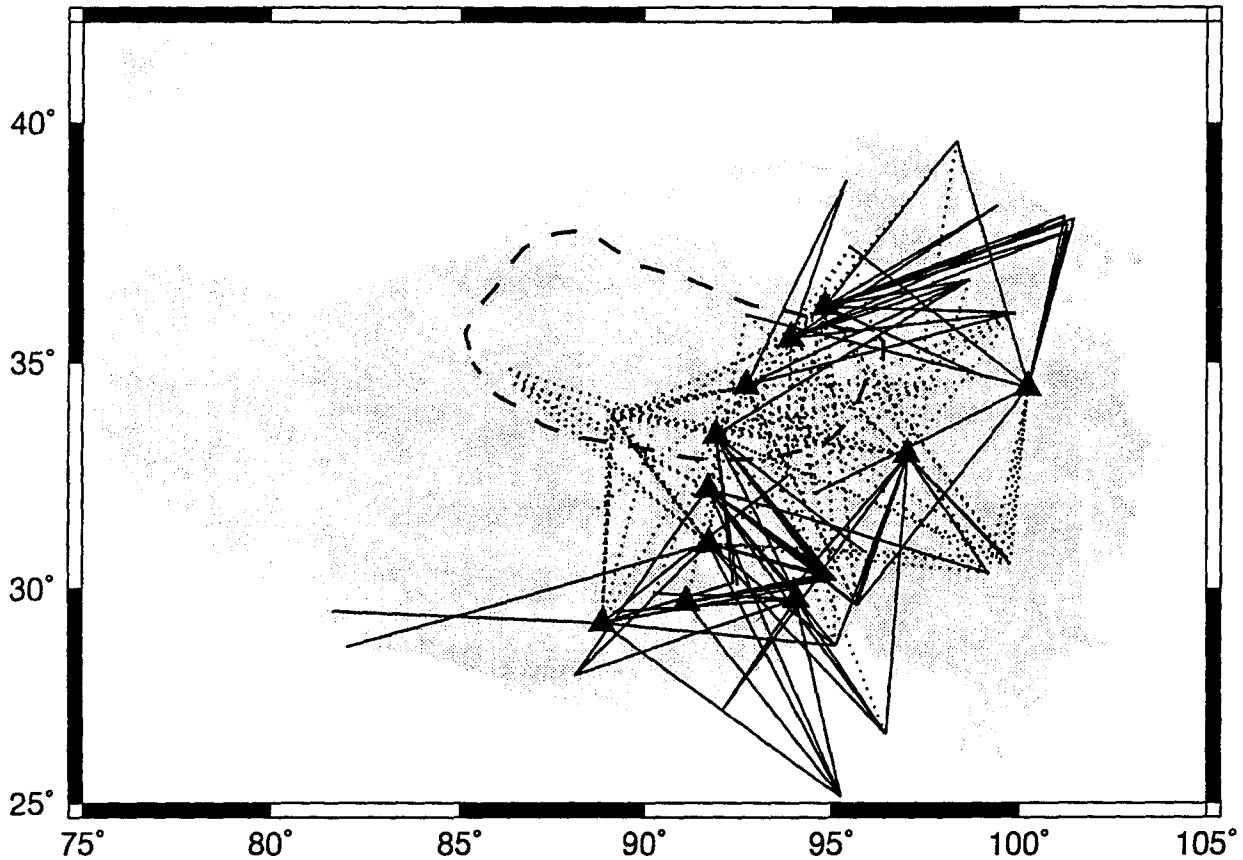


Figure 4: High-frequency S-waves propagation on the Tibet Plateau. Solid lines indicate efficient propagation paths (short-period S/P energy ratio > 0.6). Dashed lines indicate inefficient propagation paths (S/P ratio < 0.4).

The cause of the attenuation of high-frequency S-waves is not known. From the teleseismic receiver function analysis at 3 stations (TUNL, BUDO, and ERDO) located inside the attenuation zone, a mid-crustal low velocity layer is found (Zhu et al., 1995). A high Poisson's ratio was estimated in the crust under station WNDO from teleseismic P-to-S converted phase (Zhu, 1993). We suggest that there is a hot, possibly partially melted low crust in the north-central Tibet. The high attenuation of high-frequency S-waves is due to the low Q in the mid-lower crust. To demonstrate this, we plot the energy ratios of short period SH component vs. broadband SH component for all the paths within the attenuation zone and compare them with synthetic calculation for different lower crustal Q value (Figure 5). It is clear that the low Q curve (solid line in Figure 5, $Q_{\beta} = 300$) can fit the data better than high Q curve (dashed line, $Q_{\beta} = 600$).

As one more evidence for the low S-wave velocity and high attenuation in the north-central plateau, Figure 6 presents the tangential displacement records along with synthetics of one of the deep events in the southern Tibet (Event 095, Figure 1). Note that the observations at WNDO, ERDO, and BUDO are delayed about 3-5 sec relative to the synthetics. Their high-frequency amplitudes also drop compared to the stations located outside the attenuation zone (Figure 6b).

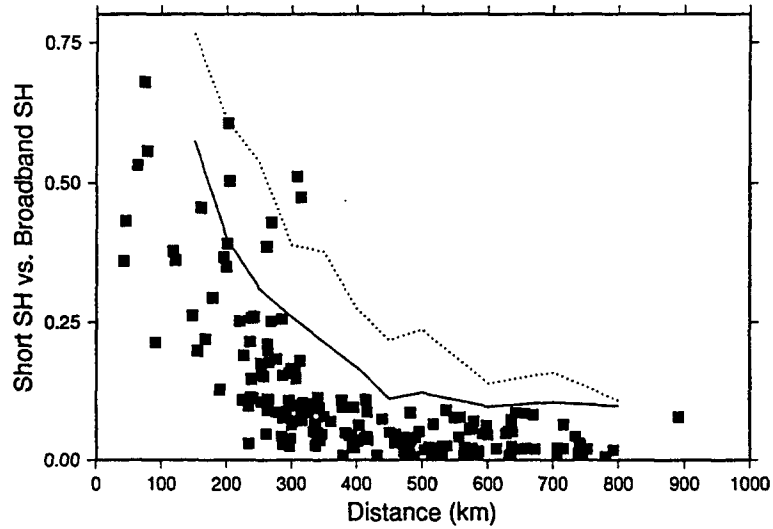


Figure 5: Energy ratios of short-period versus broadband SH component for those ray-paths within the north-central plateau. Solid and dashed lines are theoretical calculations for crustal model listed in Table 1 with different Q_{β} values in the lower crust ($Q_{\beta} = 300$ for solid line, 600 for dashed line).

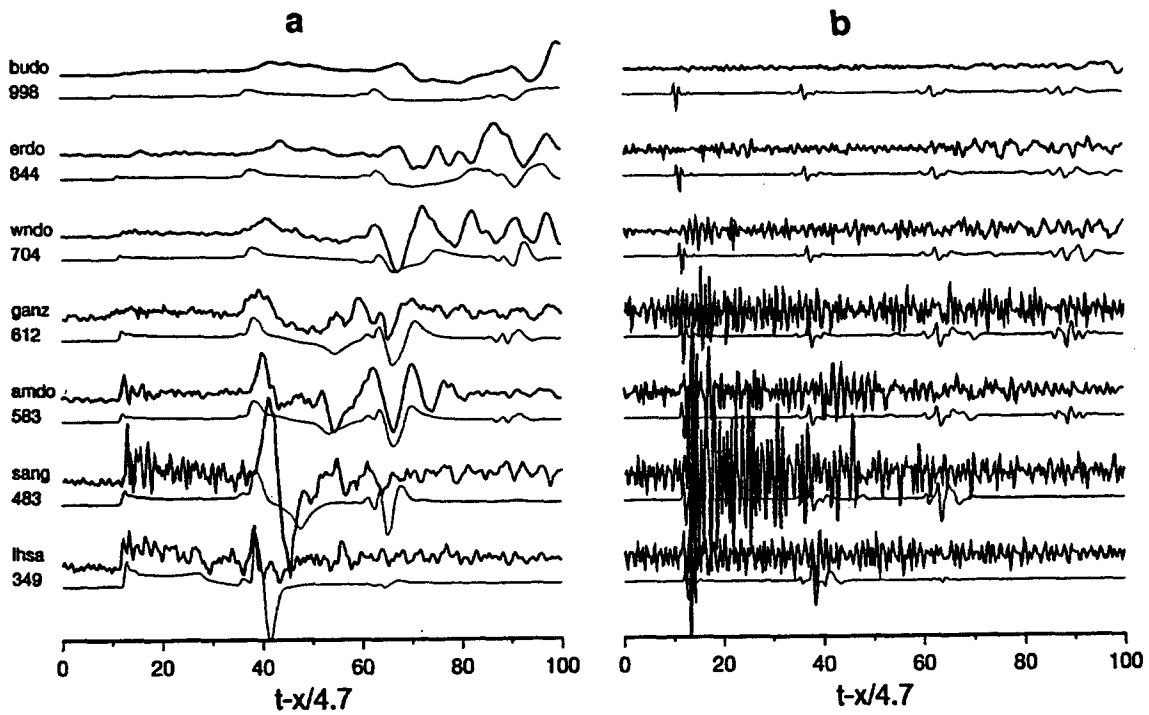


Figure 6: Broadband (a) and short-period (b) tangential displacements of event 095 (focal depth at 70 km). Traces are plotted in the same way as in Figure 3

3 CONCLUSION AND RECOMMENDATIONS

We have established an essentially good 1-D crustal model for the Tibetan Plateau. By applying improved source estimation technique to the regional events on the plateau, we have obtained their focal depths and mechanisms. Because the new method takes fully advantage of the source radiational information imbedded in the different portions of the waveforms, it will help to constrain the focal mechanisms even when only a few station records are available.

Strong variation of propagation efficiency of high-frequency S-waves exists through the plateau. In particular, there is a high attenuation zone in the north-central plateau. From the synthetic modeling and combining other evidences such as low crustal shear velocity and higher Poisson's ratio, it is suggested that the cause of the inefficient propagation of high-frequency S-wave in the north-central plateau is due to the low Q in the lower crust.

4 REFERENCES

- Harison, T.M., P. Copeland, W.S.F. Kidd, and A. Yin, 1993, Raising Tibet, *Science* 255, 1663-1670
- Molnar, P., 1988, A review of geophysical constraints on the deep structure of the Tibetan Plateau, The Himalaya and the Karakoram, and their tectonic implications, *Phil. Trans. R. Soc. Lond.* A326, 33-88.
- Ni, J. and M. Barazangi (1983). High-frequency seismic-wave propagation beneath the Indian shield, Himalayan arc, Tibetan Plateau and surrounding regions – high uppermost mantle velocities and efficient Sn propagation beneath Tibet. *JGR* 72, 665-689.
- Owens, T. J., G. E. Randall, F. T. Wu and R. S. Zeng, 1993, PASSCAL instrument performance during the Tibetan plateau passive seismic experiment, *Bull. Seism. Soc. Am.* 83, 1959-1970.
- Zhao, L. and D. V. Helmberger, 1994, Source estimation from broadband regional seismograms, *BSSA* 84, 91-104.
- Zhu, L., R. S. Zeng, F. T. Wu, T. J. Owens, and G. E. Randall, 1993, Preliminary study of crust-upper mantle structure of the Tibetan Plateau by using broadband teleseismic body waveforms, *Acta Seism. Sinica* 6, 305-315.
- Zhu, L., 1993, Estimation of crustal thickness and V_p/V_s ratio beneath the Tibetan Plateau from teleseismic converted waves (abstract), *EOS, Tran.* 74.
- Zhu, L., T.J. Owens, and G.E. Randall, 1995, Lateral Variation in Crustal Structure of the Northern Tibetan Plateau Inferred from Teleseismic Receiver Functions, *BSSA*, in press.
- Zhu, L. and D.V. Helmberger, 1995, Intermediate Depth Earthquakes beneath the India-Tibet Collision Zone, submitted to *Geophys. Res. Lett.*